ELSEVIER

Journal of Crystal Growth 230 (2001) 188–194

JOURNAL OF CRYSTAL GROWTH

www.elsevier.com/locate/jcrysgro

Solidification in Bridgman configuration with solutally induced flow

F.Z. Haddad[a], J.P. Garandet[b], D. Henry[a], H. BenHadid[a,c,*]

[a] *Laboratoire de Mécanique des Fluides et d'Acoustique, Ecole Centrale de Lyon/UCB Lyon 1, UMR CNRS 5509, ECL, BP 163, 69131 Ecully Cedex, France*

[b] *Commissariat à l'Energie Atomique, DTA/CEREM/DEM/SPCM/LRBS, CEA Grenoble, 17 rue des martyrs, 38054 Grenoble Cedex 9, France*

[c] *Université de Lyon1/Ecole Centrale de Lyon, 43 Boulevard du 11 novembre 1918, 69622 Villeurbanne Cedex, France*

Abstract

The purpose of this paper is to examine the effect of solutally induced flow on segregation during a solidification process. An idealized horizontal Bridgman configuration with moving, planar solid–liquid interface has been numerically simulated.

Solutally induced flows are first described, before analysing axial and radial segregations. It is found that in the "convective" range, segregation results compare very well with power laws obtained in the frame of an order of magnitude analysis..

Keywords: A1. Computer simulation; A1. Segregation; A1. Solutally induced flows; A2. Bridgman solidification

1. Introduction

The study of solute segregation in alloy crystals grown from the melt has been a topic of intensive research in the past 20 years, in connection with the development of numerical methods. Since the pioneering works of Brown and co-workers in the eighties (see e.g. [1,2]), a number of papers have been published on the subject, and it can be stated that the understanding of segregation phenomena is satisfying for dilute alloys. Such is not the case for concentrated systems, where the coupling between the concentration and velocity fields makes matters much more complex.

The problem has mostly been studied in the vertical Bridgman configuration in situations where the rejected solute is heavier [2,4] or lighter [3,4] than the fluid matrix. In the former case, a stratification takes place, which can significantly reduce the convection velocity, up to a point where diffusion controlled mass transport conditions prevail, as shown experimentally [5,6]. On the other hand, a thermally stable configuration will become unstable at a given threshold if a lighter solute is rejected at the interface. Even if the density gradient is globally statically stable, convective motion may appear due to the large difference between the heat and mass transfer time scales [7].

*Corresponding author. Laboratoire de Mecanique des Fluides et d'Acoustique, Ecole Centrale de Lyon/UCB Lyon 1, UMR CNRS 5509, ECL, BP 163, 69131 Ecully Cedex, France. Tel.: +33-4-72441005.

E-mail address: benhadid@mecalpha.univ-lyonl.fr (H. BenHadid).

0022-0248/01/$ - see front matter
PII: S0022-0248(01)01355-0

Our focus in the present work is to examine the effect of fluid flow on segregation in an idealized horizontal Bridgman configuration. We shall only focus on composition driven bulk natural convection, and neglect the effect of thermal convection. For the sake of simplicity, the coupling of the transport phenomena with the phase diagram, that can lead to a significant deformation of the solid–liquid interface, will not be considered. As done in previous works [8,9], our approach features a coupled numerical modeling-scaling analysis approach. Such an approach allows to identify the dominant solute transport modes in the melt and to propose relations between segregation and process parameters that can be used as rule of thumb estimates by the crystal grower.

2. Numerical model

We consider the directional solidification of a concentrated binary alloy. The melt is considered Newtonian, incompressible and obeys Boussinesq approximation. The studied configuration is schematically represented in Fig. 1 and corresponds to a cavity of aspect ratio $A = L/H$ where L is the length of the cavity and H its height. The crystal-fluid interface is supposed to be planar. The governing equations are Navier–Stokes equations coupled to those of species conservation. We use the vorticity-stream function formulation which is appropriate for the case of two-dimensional flows.

The motions are considered to be only solutally induced so that the density variation is written as

$$\rho = \rho_0[1 + \beta_c(C - C_0)],$$

where β_c is the solutal expansion coefficient, C_0 is the initial solute concentration in the melt and ρ_0 is the density related to C_0.

Let the reference variables be H for distance, v/H for velocity, H^2/v for time, and C_0 for concentration (v is the kinematic viscosity of the melt).

The domain containing the melt varies during the solidification process. We transform it in a fixed domain using the following transformation: $x = X/S(t)$ and $z = Z$, where $S(t)$ is the dimensionless length of the liquid area. According to these transformations, the dimensionless governing equations in the liquid phase are then written as

$$\frac{\partial\zeta}{\partial t} + (u - xv_i)\frac{1}{S}\frac{\partial\zeta}{\partial x} + w\frac{\partial\zeta}{\partial z} = \frac{1}{S^2}\frac{\partial^2\zeta}{\partial x^2} + \frac{\partial^2\zeta}{\partial z^2} + \mathrm{Gr_s}\frac{1}{S}\frac{\partial c}{\partial x},$$

$$\frac{1}{S^2}\frac{\partial^2\psi}{\partial x^2} + \frac{\partial^2\psi}{\partial z^2} = -\zeta,$$

$$\frac{\partial c}{\partial t} + (u - xv_i)\frac{1}{S}\frac{\partial c}{\partial x} + w\frac{\partial c}{\partial z} = \frac{1}{\mathrm{Sc}}\left[\frac{1}{S^2}\frac{\partial^2 c}{\partial x^2} + \frac{\partial^2 c}{\partial z^2}\right],$$

where ζ, ψ and c are the dimensionless variables for, respectively, the vorticity, the stream function, and the concentration. The convective velocity components u and w are defined as: $u = \partial\psi/\partial z$ and $w = -\partial\psi/\partial x$; v_i is the dimensionless solid–liquid interface velocity, so that: $v_i = V_i H/v$. The governing equations feature the non dimensional numbers of solutal Grashof, $\mathrm{Gr_s} = g\beta_c C_0 H^3/v^2$, Prandtl, $\mathrm{Pr} = v/\kappa$ and Schmidt, $\mathrm{Sc} = v/D$ (κ and

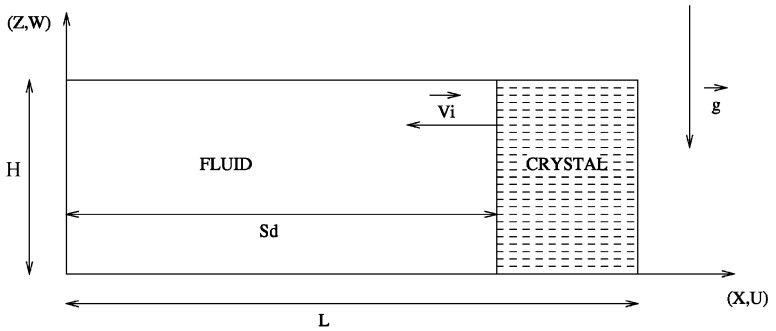

Fig. 1. Studied configuration.

D are, respectively, the thermal diffusivity and the mass diffusion coefficient). To these basic equations, need to be added the equations related to the boundary conditions.

At any instant, the amount of solute being incorporated in the solid is taken to be proportional to the amount of solute in the melt at the interface, so that

$$c_s = kc_l.$$

k is the equilibrium partition ratio (k will be fixed to the value 0.087 throughout the study), the indices s and l, respectively, relate to the solid and liquid phases. The balance equation of mass conservation at the solid–liquid interface is written as

$$\frac{\partial c}{\partial x} = \mathrm{Pe}(1-k)c$$

where Pe is the Péclet number: $\mathrm{Pe} = HV_i/D$. The other boundaries of the melt are supposed to be solid and impermeable. The mesh used is generated by Thompson technique [10]. The nodes are squeezed near the walls of the cavity and especially in the vicinity of the solid–liquid interface because of high composition gradients there. The problem is solved by using a Hermitian finite difference method with an alternative implicit direction scheme in a grid of 25×101 points on (z, x) directions [11,12]. In our numerical computations, a cavity of aspect ratio $A = 4$ is used and the solidification was conducted over the first half of the cavity.

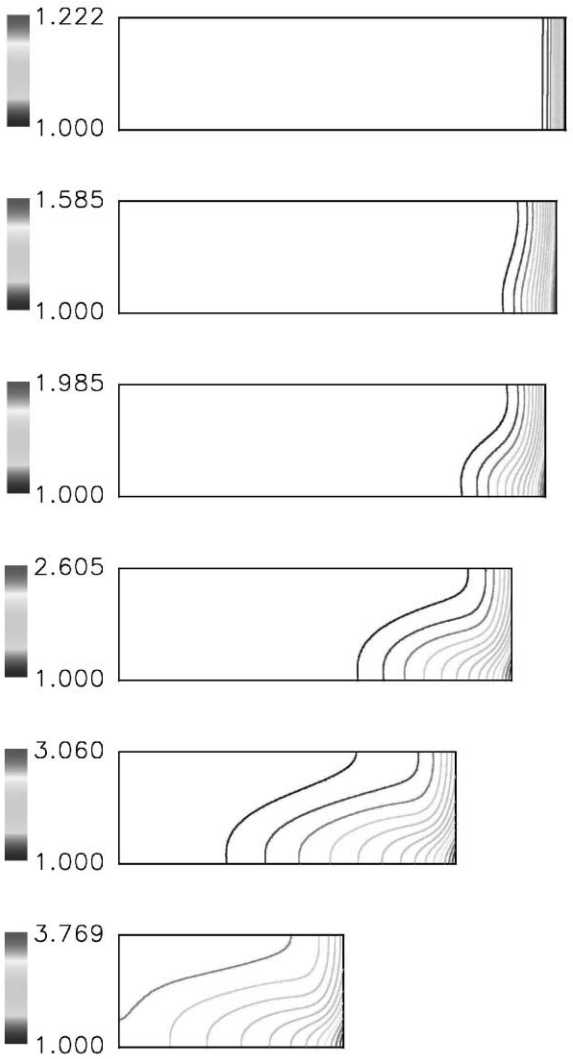

Fig. 2. Iso-concentration lines for $\mathrm{Gr_s} = 10^3$ during solidification: $S = 3.98, 3.90, 3.80, 3.50, 3.0$ and 2.0.

3. Results

3.1. Convective flow

The behaviour at low to moderate solutal Grashof numbers (typically from $\mathrm{Gr_s} = 1000$ to $\mathrm{Gr_s} = 10\,000$) is presented in Figs. 2 and 3 for the case $\mathrm{Gr_s} = 1000$. Initially, a symmetrical convective cell can be observed close to the growth interface. This can be easily understood from the fact that the composition gradients are zero away from the growth front. The corresponding isoconcentration lines are almost vertical. The continuous rejection of solute leads to an increase of interface concentration, and thus of the associated concentration gradients. Consequently, the intensity of convective motion becomes larger, and the cell gradually spreads over the whole cavity while losing its initial symmetry. Other interesting features are that the isoconcentration lines become significantly distorted, and that, even though a spreading takes place, they remain more closely packed in the vicinity of the growth front. At higher values of the solutal Grashof number

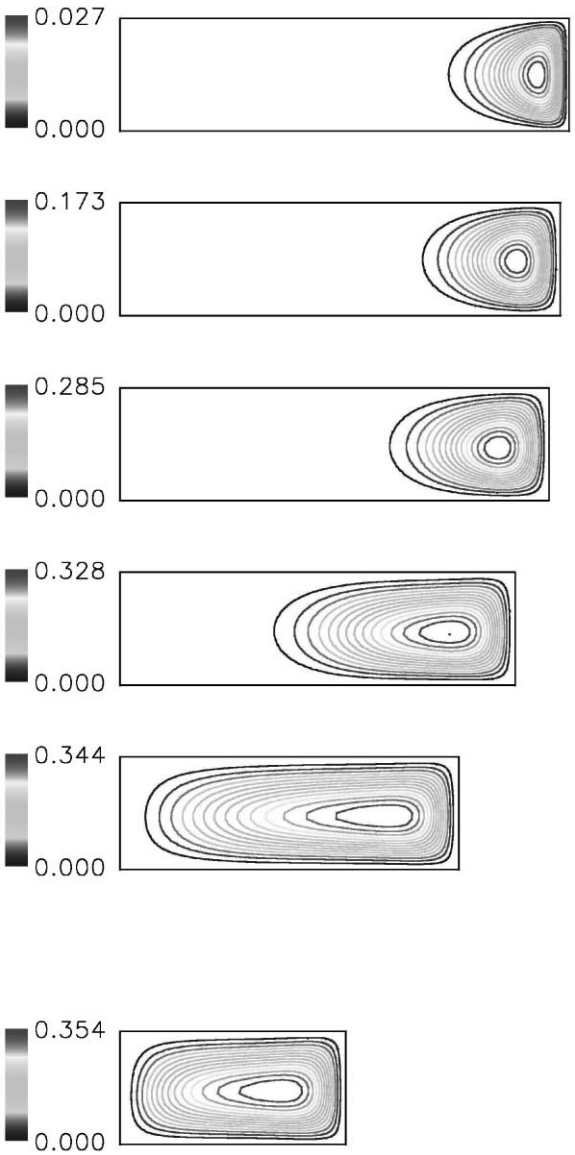

Fig. 3. Streamlines for $Gr_s = 10^3$ during solidification: $S = 3.98, 3.90, 3.80, 3.50, 3.0$ and 2.0.

(typically $Gr_s = 450\,000$, as in Figs. 4 and 5), the loss of symmetry and the spreading of the convective cell over the whole cavity take place very quickly. The flow intensity goes through a transient phase where it increases strongly, then decreases before reaching a quasi steady plateau value. A secondary cell, centered far away from

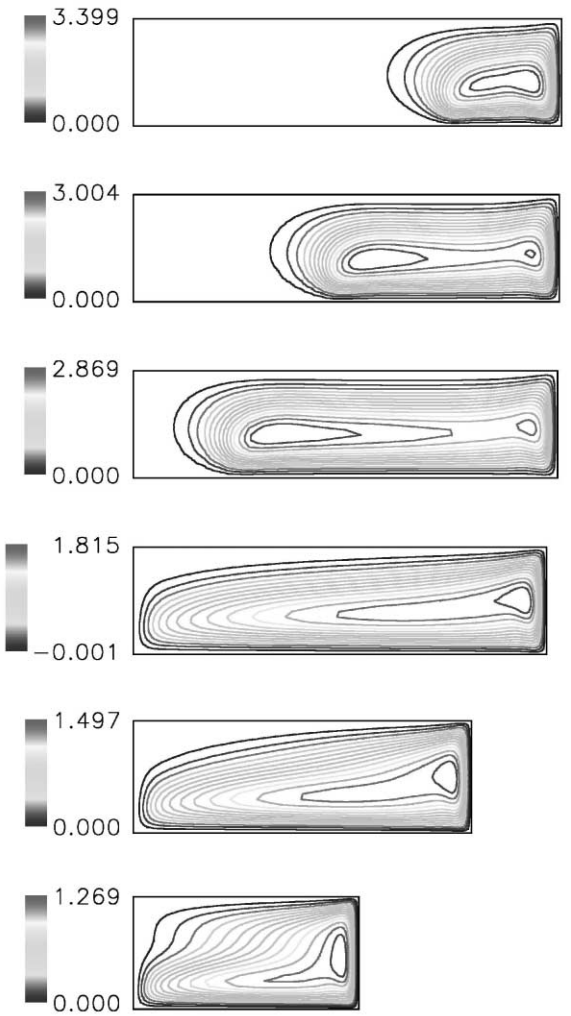

Fig. 4. Streamlines for $Gr_s = 4.5 \times 10^5$ during solidification: $S = 3.98, 3.96, 3.94, 3.84, 3.0$ and 2.0.

the interface is generated, but the primary cell, associated with the solute rejection gradients can still be observed. Regarding isoconcentration lines, the striking feature is the stratification of the liquid away from the interface, while the composition gradients remain mostly horizontal in the vicinity of the growth front.

3.2. Segregation

Axial segregation, denoted *Cl*, is classically measured by taking a solid state composition

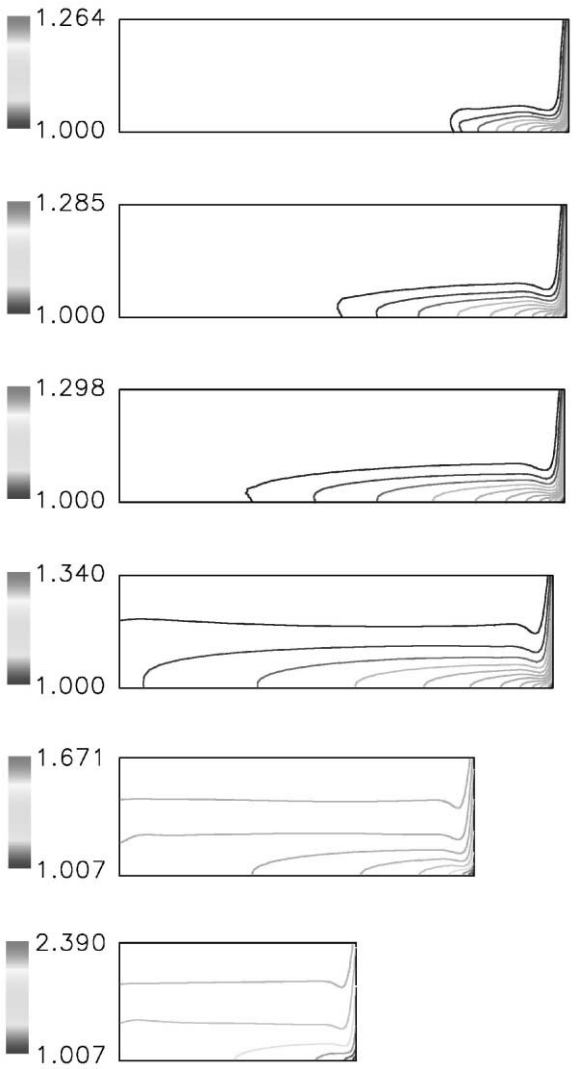

Fig. 5. Iso-concentration lines for $Gr_s = 4.5 \times 10^5$ during solidification: $S = 3.98, 3.96, 3.94, 3.84, 3.0$ and 2.0.

average over the growth interface, as:

$$Cl = c_{s\,aver}(S) = \frac{1}{C_0}\int_0^H C_s(Z, S)\,dZ. \quad (1)$$

Initially, $C_s = kC_0$, as the first solid is formed from a melt of uniform composition C_0; C_s then increases continuously, the aspect ratio of the cavity being too small for a steady state to be reached. Typical segregation curves given as a function of the solidified length are shown in Fig. 6

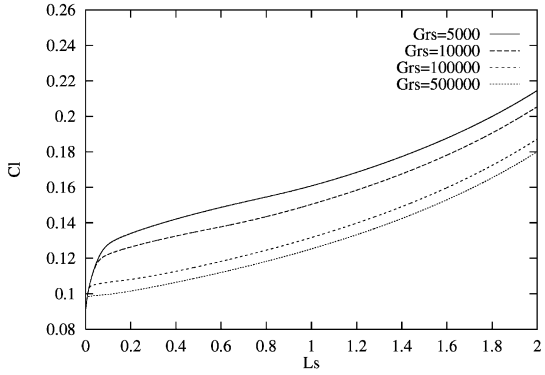

Fig. 6. Axial segregation for different Gr_s.

for various values of the solutal Grashof number, the Péclet and Schmidt numbers being fixed at $Pe = 2$ and $Sc = 10$, respectively. The effect of fluid flow is clearly apparent on the composition profiles. These curves can be interpreted in the frame of a theoretical model developed by Favier [13] that features a single non-dimensional number, namely the convecto-diffusive parameter Δ in addition to the partition coefficient. This convecto-diffusive parameter ranges from zero for convection dominated mass transport conditions to one for diffusion controlled solute transport. Favier's model was found to adequately account for axial segregation phenomena in the case of temperature driven natural convection [14]. An interesting feature of the present work was to check to which extent a quasi-steady model, such as Favier's, could account for growth conditions where the convection driving force varies continuously. Our findings are that at low Gr_s numbers (typically $Gr_s < 5000$), where both diffusion and convection are found to contribute to solute transport, the composition profiles cannot be accounted for through a single value of the convecto-diffusive parameter. On the other hand, at high convection levels typical of most growth conditions, Favier's model allows to accurately fit the segregation curves. It is only in that convective range that our results will be discussed in the next section.

Regarding radial segregation, it is measured by taking the difference between the composition maximum and minimum along the interface, normalized by the average composition

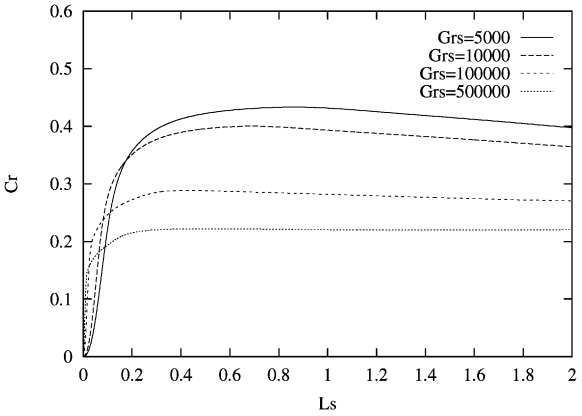

Fig. 7. Radial segregation for different Gr_s.

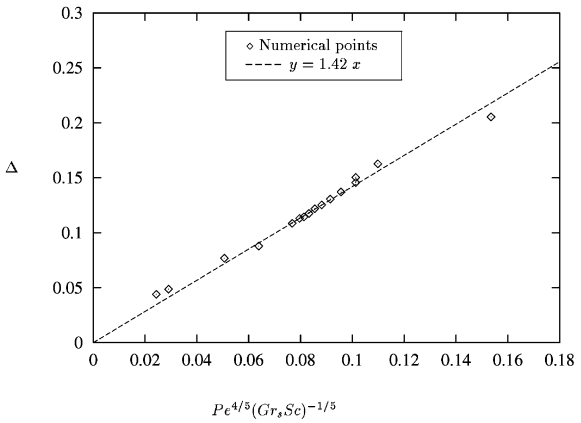

Fig. 8. Variation of Δ as a function of Pe, Gr_s and Sc under the analytical model law.

of C_s, namely

$$Cr = Cr(S) = \frac{c_{s\,max}(S) - c_{s\,min}(S)}{c_{s\,aver}(S)}. \quad (2)$$

Initially, Cr is zero since the melt composition is homogeneous; it then increases during an initial transient and reaches a relatively well defined plateau ΔC, as can be seen in Fig. 7, where a number of segregation curves obtained at various values of Gr_s are represented, the Peclet and Schmidt numbers being again fixed at $Pe = 2$ and $Sc = 10$. The plateau level decreases with increasing Gr_s, which can be qualitatively explained stating that a strong convective flow results in a well mixed liquid cavity, even in the vicinity of the growth interface. In any case, ΔC is a relevant measure of the radial segregation and as such will be used in the discussion of the next section.

4. Discussion

A number of test cases were simulated, Gr_s, Sc and Pe, respectively, ranging from 10^3 to 5×10^5, 5 to 50 and 0.5 to 4. An interesting feature of the results is that they can be interpreted in the frame of an order of magnitude analysis. Such an analysis, outlined in Ref. [15] will be presented in detail in a future paper. Regarding the convecto-diffusive parameter Δ, an equilibrium between horizontal diffusion and convection terms taken at the solutal boundary layer scale in the asymptotic convective regime yields a relation of the form:

$$\Delta \sim Pe^{4/5}(1-k)^{-1/5}(Gr_sSc)^{-1/5}. \quad (3)$$

Recalling that the partition coefficient k was kept constant in the frame of the present paper, our numerical results are plotted in Fig. 8 in a $(\Delta, Pe^{4/5}(Gr_sSc)^{-1/5})$ frame. As for radial segregation, the scaling analysis is based on an equilibrium between convective transport along the growth interface and horizontal diffusion in the bottom right corner of the liquid cavity, leading to:

$$\Delta c = \frac{\Delta C}{C_0} \sim (Pe(1-k))^{13/15}(Gr_sSc)^{-2/15}. \quad (4)$$

The numerical results are summarized in a $(\Delta c, Pe^{13/15}(Gr_sSc)^{-2/15})$ frame in Fig. 9. For both convecto-diffusive parameter and radial segregation, the agreement between the predictions of the above equations and numerical data is satisfying which supports the validity of the assumptions involved in the scaling analysis. An interesting point is that the scaling analysis is based on hypotheses similar to those invoked in the case of thermally driven convection [16,17], even though the composition fields seem to be quite different. This indicates that the observed stratification in the present solutally driven flow only has a limited influence on the concentration distribution in the vicinity of the growth front. On the other hand, the key feature of the segregation

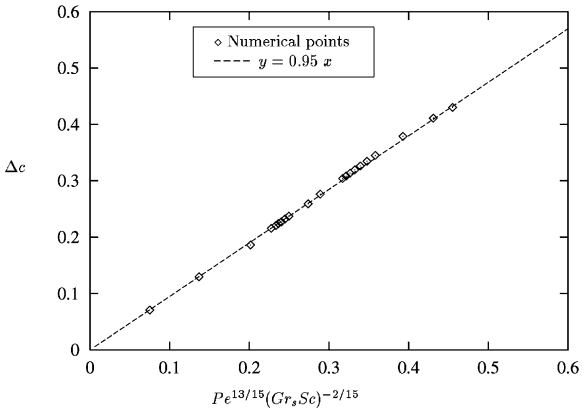

Fig. 9. Variation of Δc as a function of Pe, Gr_s and Sc under the analytical model law.

problem seems to be the existence of a solute rich boundary layer with mostly horizontal composition gradients ahead of the solid–liquid interface.

From a practical standpoint, it should be noticed that the typical values of the solutal Grashof number are often very large. Taking for instance $\beta_c = 0.001(\%^{-1})$, $g = 10\,\mathrm{m\,s^{-2}}$, $C_0 = 1\%$, $k = 0.1$, $\nu = 3\times10^{-7}\,\mathrm{m^2\,s^{-1}}$, we get $Gr_s = 10^5$. As the Schmidt number is also generally quite large (say in the 10–100 range) in metals and semiconductors, this means that mass transport will be dominated by convection. However, in an actual growth experiment, temperature gradients are also present and it is necessary to model their effect. As a matter of fact, one of the interests of the present work is to allow a comparison of the effects of thermal and solutal convection. Let us recall that the scaling laws identified in the thermal problem can be written as $\Delta \sim \mathrm{Pe(GrSc)}^{-1/3}$ [16] and $\Delta c \sim \mathrm{Pe}(1-k)(\mathrm{GrSc})^{-2/9}$ [17]. The thermal Grashof number is defined as:

$$\mathrm{Gr} = \beta_t g G_t H^4/\nu^2$$

where β_t and G_t, respectively, represent the thermal expansion coefficient and the applied longitudinal temperature gradient. Plugging in again typical values $\beta_t = 10^{-4}\,\mathrm{K^{-1}}$ and $G_t = 900\,\mathrm{K\,m^{-1}}$, we get $\mathrm{Gr} = 10^5$, a figure similar to that previously calculated for Gr_s. As the power law exponents are higher in the thermal problem, it can be expected that solutally driven convection will only have a limited impact on segregation in the present case. However, it could well be that at higher solutal expansion coefficients and/or nominal alloy concentration segregation will be governed by solutal effects. Similarly, close to the diffusive transport regime, i.e. in a parameter range where the above scaling analysis is not applicable, the influence of solute driven convection could be dominant. In any case, future work should focus on the coupled thermal-solutal problem to allow a definite conclusion on such a complex topic.

Acknowledgements

The contribution of J.P. Garandet is part of the MAP project "Crystallization of CdTe and related compounds" supported by the European Space Agency.

References

[1] C.J. Chang, R.A. Brown, J. Crystal Growth 63 (1983) 343.
[2] P.M. Adornato, R.A. Brown, J. Crystal Growth 80 (1987) 155.
[3] C. Le Marec, R. Guérin, P. Haldenwang, J. Crystal Growth 169 (1996) 147.
[4] W. Seifert, P. Reinshaus, A. Bachran, Cryst. Res. Technol. 33 (1998) 899.
[5] A. Rouzaud, D. Camel, J.J. Favier, J. Crystal Growth 73 (1985) 149.
[6] M.W. Price, R.N. Scripa, S.L. Lehoczky, F.R. Szofran, C.H. Su, J. Crystal Growth 198/199 (1999) 297.
[7] S.R. Coriell, M.R. Cordes, W.J. Boettinger, R.F. Sekerka, J. Crystal Growth 49 (1980) 13.
[8] S. Kaddeche, J.P. Garandet, C. Barat, H. BenHadid, D. Henry, J. Crystal Growth 158 (1996) 144.
[9] F.Z. Haddad, J.P. Garandet, D. Henry, H. BenHadid, J. Crystal Growth 204 (1999) 213.
[10] J.F. Thompson, Z. Vawarsi, C.W. Matsin, Numerical Grid Generation, Elsevier, Amsterdam, 1985.
[11] B. Roux, P. Bontoux, T.P. Loc, O. Daube, in: R. Rautmann (Ed.), Lecture Notes in Mathematics, Vol. 771, Springer, Berlin, 1980, p. 450.
[12] R. Hirsh, J. Comput. Phys. 19 (1975) 90.
[13] J.J. Favier, Acta Met. 29 (1981) 197.
[14] S. Kaddeche, H. BenHadid, D. Henry, J. Crystal Growth 135 (1994) 341.
[15] F.Z. Haddad, Ph.D. Thesis, Ecole Centrale de Lyon, 2000.
[16] J.P. Garandet, T. Duffar, J.J. Favier, J. Crystal Growth 106 (1990) 437.
[17] J.P. Garandet, J. Crystal Growth 114 (1991) 593.